GEOLOGY OF CHANG'E-3 LANDING SITE AND PATH PLANNING FOR YUTU ROVER. J. Zhao[1], J. Huang[1], L. Xiao[1], L. Qiao[1], Z. Xiao[1] and Q. Huang[1]. [1]Planetary Science Institute, China University of Geosciences, Wuhan, 430074, P. R. China (jnzhao@cug.edu.cn)

Introduction: Nearly 40 years after the completion of Apollo program and Luna missions, the third Chinese lunar mission, Chang'e 3 (CE-3), was launched on December 2 2013, and it safely landed on the surface of the Moon on December 14 2013. The rover "Yutu" separated from the lander successfully about 8 hours later. The landing site of CE-3 is 340.49 °E, 44.12 °N, located in the northern part of Mare Imbrium and about 140 km east to Sinus Iridum. The landing area has a variety of geologic features, such as impact craters, wrinkle ridges and basaltic lava flows with different ages, making it an arresting place to study.

Geological maps in Apollo era [1] and recent studies [2-4] reveal regional geologic information for Sinus Iridum and adjacent terrains. However, the spatial resolution of those maps is not sufficient for the rover path planning from both scientific and engineering requirements. Luckily, as more and more high spatial resolution remote sensing data being acquired by recent lunar missions such as Chang'e 1 & 2, SELENE-1, Chandrayaan-1 and Lunar Reconnaissance Orbiter (LRO), large scale geological mapping and detailed study are possible for CE-3 landing region. In this study, we have mapped an area of 1 °×1 ° (~660 km^2) centered near CE-3 landing site due to the mobile ability of the rover and presented topographic, elemental, and geomorphologic results of the landing region. Our results will support the future path planning and give help on selecting valuable detecting target for Yutu rover.

Methods: High-resolution DTM of the landing area is obtained from stereopair images of Terrain Camera (TC) onboard SELENE-1 [5]. Its spatial resolution is 10 m/pixel, which is better than the DEM produced from Lunar Orbiter Laser Altimeter (LOLA) data at the same studied latitudes.

FeO and TiO_2 abundances are estimated with data acquired by Multispectral Imager (MI) onboard SELENE-1 using the method developed by Otake [6]. As the spatial resolution of MI data is 20 m/pixel, we can get better results than that obtained by Clementine UV/VIS data whose average spatial resolution is 115 m/pixel and the coverage is poor in the study area.

Detailed analysis of geomorphic features is based on images of Narrow Angle Camera (NAC) and TC. The spatial resolutions of them are 0.5 m/pixel and 10 m/pixel respectively.

Results: *Topography.* The elevation of CE-3 landing site is about -2610 m. Surface topographic difference is less than 300 m for the whole study area. Middle and southern parts are higher in elevation, while the northwest and northeast are lower. Besides, 80% of the area is relatively flat (less than 5 °), only the steepest part in the inner walls of some impact craters has a slope larger than 20 °. The slope of the landing site is about 5 °, which is suitable for the exploration of the rover.

Rock types. Rock types in the two geological units (Fig. 2, Em and Im) are estimated according to the FeO and TiO_2 abundances. Unit Em (Eratosthenian mare material) has both higher FeO (17-18 %) and TiO_2 (6-12 %) abundances, while unit Im (Imbrian mare material) has lower abundances (FeO: ~15%, TiO_2: <3%). Therefore, primary rock type of unit Em is high-Ti basalt and unit Im is low to very-low basalt [7]. Some large impact craters in unit Em have lower values than their surrounding terrains, which imply that they may have dig into and exposed underlying materials of unit Im. By measuring the depths of the craters mentioned above, we could roughly estimate the thickness of basalt unit Em. Our result shows the thickness of unit Em is less than 70 m, which is in agreement with previous studies [8-9].

Geomorphic features. Impact craters in the study area are simple bowl-shape craters and relatively small in size. We divided the impact craters into four types based on degradation. Type 1 (Fig.1 Crater a) is fresh crater with bright rays. Type 2 (Fig.1 Crater b) is slightly degraded crater characterized by its round shape, relatively high depth/diameter (d/D) ratio, plenty of boulders and middle to high albedo. Type 3 (Fig.1 Crater c) is heavily degraded crater with subdued initial features and low d/D ratio and albedo. Type 4 (Fig.1 Crater d) is ghost crater that has been largely buried by lava flows.

Two types (Ridge I and II in Fig. 1) of wrinkle ridges can be recognized in this area. Ridge I is broad and smooth, with 8 km width at the bottom and 3.5 km width at the top, and a flank slope of lower than 3 °. Ridge II is narrow and contorted, with a flank slope of more than 15 °. Ridge I mainly lies in Im unit with a great number of highly degraded craters lying on its top, which implies that Ridge I is relatively old and the central part of it has been buried by lava flows that constitute Em mare basalt unit. In contrast, Ridge II stretches on both the Im and Em unit and the formation of Ridge II leading to the destruction of some relatively young craters, indicating a fairly young age of Ridge II.

Geological map and regional evolution history. Fig. 2 is the geological map of the study area. Ages of Im and Em units are 3.32 Ga and 2.50 Ga respectively according to the most recent study by Qiao [4]. Based on these age information, we proposed a scenario for geological evolution of the region. The Im unit formed about 3.32 Ga ago followed by the formation of Ridge I. Then 2.5 Ga ago, lava flows from the late-stage volcanism in Mare Imbrium formed Em unit. At last, Ridge II and some rayed craters formed in this region.

Discussion: *Formation mechanism of wrinkle ridges in the study area.* Formation of north-south ridges in Mare Imbrium can be related to the subsidence of the mare, or recent horizontal compression due to the global cooling of the Moon [10-13]. As discussed above, two types of ridges are different in age. Ridge I formed just after the formation of Im unit, so its formation mechanism may be related to the subsidence of the lunar maria. Ridge II is relatively young, and it may be the result of global late-stage contraction of the Moon.

Rover path planning. "Yutu" rover is equipped by Panorama Camera, Visible/Near Infrared Imager, Alpha Particle X-Ray Spectrometer and Ground-Penetrating Radar. These scientific instruments can be used to take images, analyze mineralogy & chemistry of the lunar surface, and identify the subsurface structure of the shallow crust. The designed working distance is 3 km around the landing site, with a total distance of 10 km. Hereafter, we propose two detecting paths for the rover.

Path 1 is suggested to explore the nearest type 1 impact crater (Fig.1 Crater e) and to reveal why the rays have different albedo from the surrounding terrains [14]. This will be the first time to provide "ground truth" for the surface albedo differences.

Path 2 is ideal to rove to the rim of Crater b and f in Fig.1. First we can study the subsurface structure of the traverse, including regolith thickness, lava flow thickness and faults. Then we are able to study the morphology of the impact crater in detail and observe the degradation. Finally, Crater f has possibly dig out the materials of Im, and it will be an opportunity to study the lower TiO_2 abundance basaltic materials and understand the magma evolution of Mare Imbrium in space and time.

Summary: We make a comprehensive analysis of the geology of CE-3 landing area. Surface morphology of the area is relatively flat. Two basalt units Em and Im are mapped. Craters in this area are divided into four types based on degradation, and two types of wrinkle ridges are observed with possible different origins. Geological map is compiled and the geological evolution history is reconstructed. Moreover, we proposed two paths for the future exploration of Yutu rover.

References: [1] Schaber G. G. (1969) *Geologic map of the Sinus Iridum quadrangle of the Moon.* [2] Chen S. et al. (2010) *Sci. China Ser. G, 53,* 2179-2187. [3] Ding X. et al. (2013) *Acta Geol. Sin.-Engl., 83,* 1643-1657. [4] Qiao L. et al. (2012) *Sci. China Ser. G, 43,* 1370-1386. [5] Haruyama J. et al. (2012) *43rd LPSC,* Abstract #1200. [6] Otake H. et al. (2012) *43rd LPSC,* Abstract #1905. [7] Neal C. R. and Taylor L. A. (1992) *GCA, 56,* 2177-2211. [8] Schaber, G. G. (1973) *4th LPSC,* 73-92. [9] Hiesinger H. (2002) *GRL, 29,* 89. [10] Lucchita B. K. (1977) *Proc. Lunar Sci. Conf. 8th,* 2691-2703. [11] Yue Z. et al. (2007) *Chin. J. Geochem., 26,* 418-424. [12] Watters T. R. et al. (2010) *Science, 329,* 936-940. [13] Daket Y. et al. (2013) *EGU2013,* Abstract #3747. [14] Hawke B. R. et al. (2004) *Icarus, 170,* 1-16.

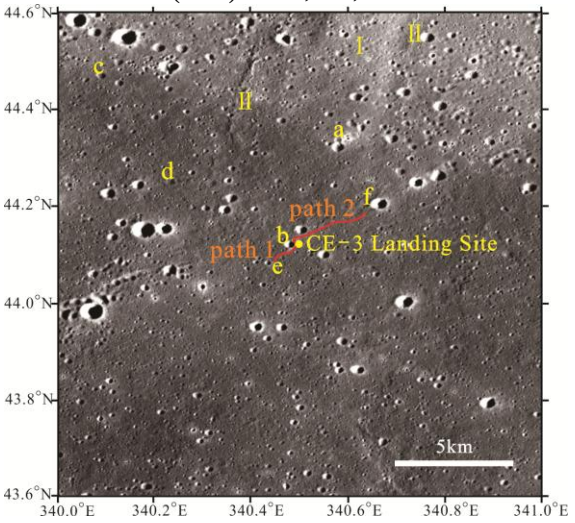

Figure 1. TC morning image of the study area (simple cylindrical projection). "a-d" are craters of different degradation degree. "e" is a rayed crater near CE-3 landing site. "f" is a crater with low TiO_2 abundance. "I" and "II" are ridges of different types. Red lines are suggested paths for Yutu rover.

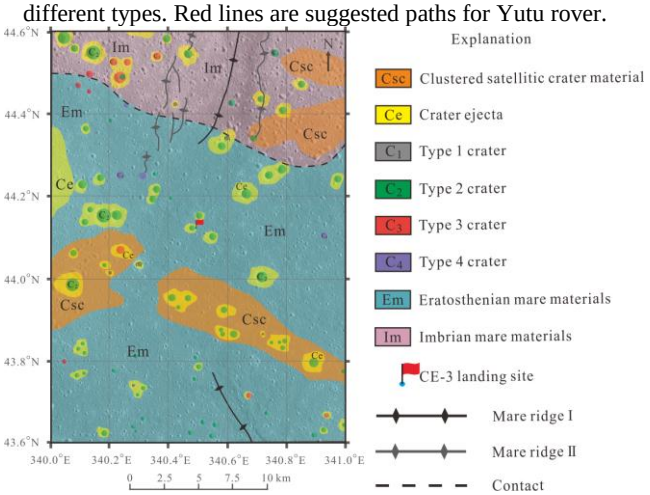

Figure 2. Geological map of the study region. Background is TC morning image given in a Lambert projection.